

Measurements of the depth of maximum muon production and of its fluctuations in extensive air showers above 1.5×10^{19} eV at the Pierre Auger Observatory

Manuela Mallamaci^{*a} for the Pierre Auger Collaboration^b

^a INFN, Sezione di Milano, Italy

^b Observatorio Pierre Auger, Av. San Martín Norte 304, 5613 Malargüe, Argentina

E-mail: auger_spokespersons@fnal.gov

Full author list: http://www.auger.org/archive/authors_icrc_2017a.html

The surface detector array of the Pierre Auger Observatory measures the arrival time distribution of particles, providing indirect information on the longitudinal development of the muonic component of extensive air showers. In this work, the depth at which the muon production is maximum and the corresponding fluctuations are reconstructed for more than 2000 events above 1.5×10^{19} eV, in a wide range of zenith angles, between 45° and 65° . Both observables are exploited to gain insight about the most up-to-date hadronic interactions models, which are used in the simulation of extensive air showers. By constraining the models, these observables could allow one to obtain better information on high energy hadronic interactions, and therefore they could indirectly help for the mass composition study of ultra-high energy cosmic rays, one of the most intriguing issues of modern astrophysics.

*35th International Cosmic Ray Conference — ICRC2017
10–20 July, 2017
Bexco, Busan, Korea*

*Speaker.

1. Introduction

In recent decades, the advent of detectors reaching apertures as large as tens of thousands $\text{km}^2 \text{ sr yr}$ have significantly improved our knowledge of the Ultra-High Energy Cosmic Rays (UHECRs). Among the most significant results, the extremely precise measurement of the UHECR flux at the Pierre Auger Observatory has to be mentioned [1]. Also our understanding of mass composition of UHECRs makes a considerable progress. In particular, the data taken by the Fluorescence Detector (FD) at the Pierre Auger Observatory have shown a trend from a light composition at the ankle of the spectrum to a heavier one for increasing energies [2, 3]. This conclusion is reinforced by exploiting Surface Detector (SD) data analyses [4] and by correlations among different observables measured by both FD and SD [5]. In this context, it has to be mentioned that the interpretation of the results depends crucially on the Monte Carlo simulation of Extensive Air Showers (EAS) and therefore on the accuracy of the modeling of hadron-air collisions at high energies. Even if a considerable progress has been done [6], the reliability of EAS simulations is the largest source of systematic uncertainty in the determination of the mass composition of UHECRs.

In this work, the SD has been exploited to reconstruct the so-called *Muon Production Depth* (MPD), i.e. the longitudinal profile of muons produced in EAS. The MPD turned out to be meaningful, being sensitive to the primary composition and in particular to the details of hadronic interactions. This is the reason why it is considered a potential tool for constraining the models used for the simulation of EAS [6, 7].

A first analysis of the MPD was performed in [8], considering events above 2×10^{19} eV, arriving with large zenith angles ($55^\circ \leq \theta \leq 65^\circ$) and considering stations far from the shower core ($r > 1700\text{m}$), where the electromagnetic component is almost completely absorbed.

In the present work, a new method is used to reconstruct the MPD on a wider range of energies, arrival directions and distances from the shower core [9, 10]. It will be discussed in Sec. 2, focusing on the evaluation of X_{max}^μ , i.e. the atmospheric depth at which the muon production rate reaches a maximum in EAS, and on the corresponding fluctuations. The results on data will be presented in Sec. 3.

2. Reconstruction of the distribution of the muon production depths

The time structure of the muonic component of a shower can be exploited to obtain the distribution of muon production distances along the shower axis. This carries information about the nature of the primary UHECR and about the longitudinal development of the hadronic component of the EAS. The muonic longitudinal profile is reconstructed in terms of production depth X , i.e. the total amount of traversed matter in g/cm^2 . This quantity is easily related to the production height z , by taking into account the atmospheric density profile $\rho(z)$:

$$X(z) = \int_z^\infty \rho(z') dz' \quad (2.1)$$

For each UHECR event, the set of depths X where muons are produced forms the MPD distribution. It has to be underlined that only muons surviving the passage through the atmosphere can be detected at ground. Therefore, the so-called *apparent* MPD profile will be measured. The maximum of this distribution is X_{max}^μ .

In this work, the MPD is reconstructed for EAS arriving with zenith angle $45^\circ \leq \theta \leq 65^\circ$, for energies larger than 1.5×10^{19} eV and considering all muons arriving at radial distances from the shower core $r > 1200$ m. Considering the above mentioned ranges and the realistic measurement conditions, the reconstruction of the MPD is a combination of different ingredients [9, 10], which are summarized below.

- The electromagnetic component must be removed in order to isolate the muonic signal in the FADC traces recorded by the SD stations. This step is mandatory, because of the significant contamination affecting especially events with low zenith angles. The background removal is implemented by means of a smoothing algorithm, based on the difference between the spiky structure of the muonic signals as compared to the smoother electromagnetic ones. In addition, a time cut on recorded traces allows one to get rid of the unavoidable background of high energy γ -rays ($E > 300$ MeV). These procedures are both applied on FADC traces recorded by the SD stations with $r > 1200$ m. This choice is related to the next point.
- Once the muonic signal is extracted, the production depth X must be evaluated. This is obtained by using a theoretical model developed in [11]. According to simple assumptions, the equation for the production height, z , is derived:

$$z = \frac{1}{2} \left(\frac{r^2}{ct_g} - ct_g \right) + \Delta - \langle z_\pi \rangle \quad (2.2)$$

t_g is the time delay of muons with respect to a shower front plane traveling at light speed, Δ is the distance from the shower front plane to the muon impact point at ground and $\langle z_\pi \rangle$ is the pion decay length. t_g , the *geometric delay*, is given by $t_g \simeq t - t_\epsilon$, where t is the total delay measured by the SD and t_ϵ is the *kinematic delay* due to the sub-luminal muon velocities. This quantity must be parametrized, as the SD does not measure particle energies. In this work, a parametrization based on the post-LHC hadronic interaction models, QGSJetII-04/EPOS-LHC, is used. It takes into account the dependence of t_ϵ on the zenith angle θ , on the radial distance r and on the muon production height z . At ground level, a limited range of core distances must be considered to keep the contribution of the kinematic delay low. A cut for $r < 1200$ m ensures $t_\epsilon < 0.2 t_g$.

By simulating the reconstruction conditions, it has been found that the MPD profiles are distorted by detector effects, like the light propagation inside the detector and the electronics response. These effects smear the muon arrival times, causing an uncertainty which results in an uncertainty in X and therefore in a distortion of the reconstructed MPD distribution. This can be compensated on average by subtracting to each time bin a global time offset, $T_{shift} = 60$ ns. Its value is independent of energy and zenith angle and it is related to the decay time of the muon signal in the SD station [9, 10].

- For each event, the reconstructed MPD profile is fitted by means of the Universal Shower Profile (USP) function [12]:

$$\frac{1}{N} \frac{dN}{dX} = \left[1 + \frac{R}{L} (X - X_{\max}^\mu) \right]^{R-2} e^{\left(-\frac{X - X_{\max}^\mu}{LR} \right)} \quad (2.3)$$

X is the slant depth defined by Eq. (2.1) and there are four parameters: N is the number of muons, X_{\max}^{μ} is the point along the shower axis where the muon production reaches its maximum, L represents the profile width and R quantifies the deformation of the profile with respect to a Gaussian distribution. The best set of parameters is obtained through a log-likelihood minimization of the USP function. Because of the discrete sampling (the SD stations are indeed separated by 1.5 km and have a finite collecting surface; in addition we select stations with $r > 1200$ m from the core), the number of muons is much lower than in the ideal case and this limits the efficiency of the estimation of X_{\max}^{μ} with a free parameter fit. The asymmetry parameter R is therefore fixed as a function of the zenith angle, on an event by event basis. Indeed it depends on the zenith angle, and also on the nature of the primary and the hadronic interaction model. For this reason, $R=f(\theta)$ has been determined with Monte Carlo on a mixed sample of proton/iron-induced showers, based on QGSJetII-04/EPOS-LHC. A second reconstruction based on a more flexible fit has been used to estimate the possible systematic uncertainty by such optimization.

- A set of selection cuts is used in order to have a sample of well-reconstructed events. First of all, only fully contained events are considered, by requiring that the SD station with the highest signal be surrounded by six closest and fully operational neighbors. In addition, at least 5 stations with signal larger than 3 VEM (Vertical Equivalent Muon) are required to contribute to the reconstruction. This avoids trigger fluctuations and minimizes the impact of accidental signals. Finally, a set of quality criteria is applied after the fit procedure. In particular, for converging fits, L is required to be between 130 and 415 g/cm², a range chosen as a three-sigma limit on its distribution for both data and Monte Carlo simulations. This allows one to discard events for which the MPD distribution is not well reconstructed in the first part or in the tail, leading to unphysical values for the parameter L . In addition, events with a relative uncertainty $(\delta X_{\max}^{\mu} \times \sqrt{\chi_*^2})/X_{\max}^{\mu} \geq \epsilon_{\max}$ are rejected, where δX_{\max}^{μ} and χ_*^2 are respectively the error on the parameter and the reduced χ^2 of the fit. ϵ_{\max} goes from 28% to 18%, depending on the energy, since the reconstruction improves with it, and its value is chosen as a three-sigma limit on the $(\delta X_{\max}^{\mu} \times \sqrt{\chi_*^2})/X_{\max}^{\mu}$ distribution, obtained on a mixed sample of proton/iron-induced showers. The overall selection efficiency, i.e. the number of events which pass the quality criteria, is larger than 90% (on both data and simulations) and the difference in efficiency between proton and iron simulated events is smaller than 5% at all energies, zenith angles, and for both hadronic interaction models.

Fig. 1 shows a typical simulated MPD histogram, after the reconstruction procedure here described. The USP fit is superimposed and the reconstructed maximum is indicated in the inset of the figure as $X_{\max}^{*\mu}$. The performances of the reconstruction have been evaluated on Monte Carlo by defining a *bias*, as the difference $(X_{\max}^{*\mu} - X_{\max,MC}^{\mu})$, where $X_{\max}^{*\mu}$ is the MPD maximum reconstructed with all the ingredients listed above, and $X_{\max,MC}^{\mu}$ is instead obtained at the generation level (i.e. in the ideal condition in which X is a known quantity). The bias and the corresponding resolution of the measurement are reported in Fig. 2 (respectively left and right panel) as a function of the primary energy, for a set of proton and iron-induced showers simulated with CORSIKA and QGSJetII-04/EPOS-LHC models [9, 10]. By looking Fig. 2 (left), one can see how the reconstruction depends on the primary mass and hadronic model. This mass/model-dependent performance is due to a

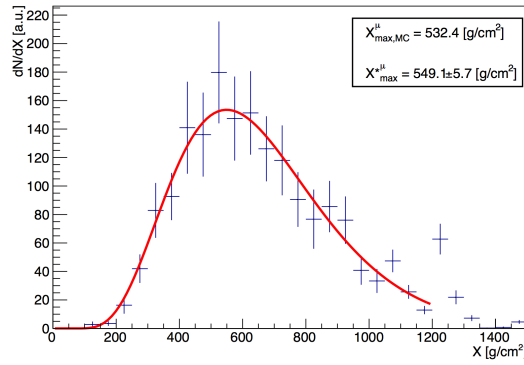


Figure 1: Example of a MPD distribution and USP fit (red line) for an iron-induced air shower simulated with CORSIKA and EPOS-LHC model, $\log_{10}(E/\text{eV})=19.65$, $\theta = 55^\circ$. The MPD is determined through complete shower simulation and reconstruction, using Auger Offline software and the procedure described in Sec. 2 (see text for the details). The inset shows the values for $X_{\text{max,MC}}^{\mu}$ and $X_{\text{max}}^{*\mu}$, which are respectively obtained at generation level and after the reconstruction chain.

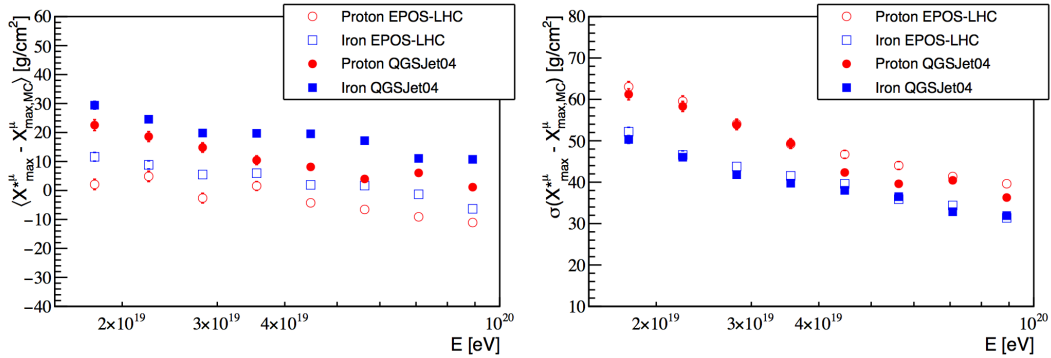


Figure 2: Average reconstruction bias of the MPD maximum (left) and resolution of the method (right) as a function of the primary energy, shown for the whole zenith angle range of this analysis [45° - 65°].

combination of factors, like the parametrization of the kinematical delay, the fitting procedure and detector effects like the time response of the SD stations. For what concerns the detector resolution, it improves with the energy and with the primary mass, as it depends especially on the number of muons at disposal for the reconstruction.

The dependence of the reconstruction on mass and hadronic models would be the largest source of systematic uncertainty: we call it *mass and model spread* and it amounts to $\pm 14 \text{ g/cm}^2$ (evaluated conservatively as the difference between the maximum and the minimum value of the bias). For this reason and given that the discriminating power of the MPD is not affected by the reconstruction (see expectations in Fig. 3), we choose to evaluate the MPD maximum folded with reconstruction effects, i.e. $X_{\text{max}}^{*\mu}$.

3. Results on data

All events recorded by the SD of the Pierre Auger Observatory between January 2004 and

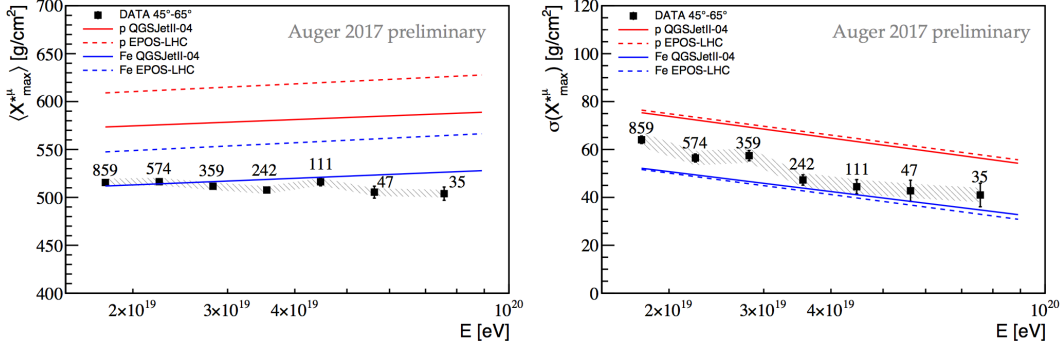


Figure 3: $\langle X_{\max}^{*\mu} \rangle$ (left) and the corresponding fluctuations (right) as a function of the primary energy. Data (black squares) are shown with statistical (black line) and systematic uncertainties (gray band) and compared to simulations (see text for the details).

December 2016 have been used in this analysis. Considering the applicability ranges of this work and the selection criteria described in Sec. 2, the number of UHECR events here analyzed is 2227. Data have been studied as a function of the primary energy. A bin width $\Delta \log_{10}(E/eV) = 0.1$ is chosen for energies $\log_{10}(E/eV)$ between 19.2 and 19.8. Not having enough statistics to keep the same binning, data are integrated in one bin for $\log_{10}(E/eV)$ in the range [19.8-20]. For each energy bin, the first two moments of the $X_{\max}^{*\mu}$ distribution are evaluated on data and are compared directly to the expectations obtained from Monte Carlo simulations after the reconstruction procedure (Sec. 2). We note that data and Monte Carlo are both equally biased by the reconstruction, so the relative distance to the reference lines does not vary in $X_{\max}^{*\mu}$ (see below conversion to the mean logarithmic mass $\langle \ln A \rangle$) and no systematics are associated to these effects. On the contrary, the physical X_{\max}^{μ} would display the mass and model spread as systematics, as discussed previously.

The overall systematic error on the first two moments of the $X_{\max}^{*\mu}$ distribution turns out to be around 4 g/cm^2 and 3 g/cm^2 respectively, and due to two sources: the small dependence of the selection efficiency of the quality cuts on the primary mass ($\simeq 1 \text{ g/cm}^2$) and the time variability of data. An additional systematic error of $\simeq 7.5 \text{ g/cm}^2$ can be associated with the event selection and procedure to fit the MPD profiles and needs to be taken into account in the determination of $\langle \ln A \rangle$ (see below). The results on $\langle X_{\max}^{*\mu} \rangle$ are shown in Fig. 3 (left) by black squares, with their statistical (black line) and systematic uncertainties (gray band). For each energy bin, the number of events is indicated. From the comparison with the predictions, the inconsistency among models and data is evident. In the case of EPOS-LHC, data are at odds with predictions for all reasonable masses, in the whole energy range. Considering instead QGSJetII-04 and in particular iron expectations, a mild incompatibility arises at the highest energies. We have also checked that when converting $X_{\max}^{*\mu}$ to X_{\max}^{μ} by using the reconstruction bias (Fig. 2 left) averaged on mass/models, we obtain a good agreement with the results shown in Fig. 3 and with results presented in [8].

The inconsistencies outlined here make it difficult to draw firm conclusions on composition with our measurement of $\langle X_{\max}^{*\mu} \rangle$: we see that the predictions of $\langle X_{\max}^{*\mu} \rangle$ from the two hadronic models are significantly different in absolute value ($\approx 35 \text{ g/cm}^2$). However, we can note that the muonic elongation rate, i.e. the rate of change of $X_{\max}^{*\mu}$ with primary energy, is predicted to be about

$\sim 25 \text{ g/cm}^2/\text{decade}$, independently of the primary mass and hadronic model, while on data we found $-16.9 \pm 7.2 \text{ g/cm}^2/\text{decade}$. We could thus interpret the elongation rate inferred from data at face value and conclude that our results appear to be in tension with a constant composition at the highest energies. Further work is however required to estimate more accurately the systematic uncertainty of the measured elongation rate.

An additional information comes from the second moment of the $X_{\text{max}}^{*\mu}$ distribution. In particular, the observed fluctuations carry information about the physical fluctuations and therefore potentially about the primary mass. The results are shown in the right panel of Fig. 3. Note that in this case, the Monte Carlo predictions for different hadronic models agree with each other, making the second moment less hadronic model dependent. The energy dependence is due to the detector resolution, being $\sigma^2(X_{\text{max}}^{*\mu}) = \sigma_{\text{phys}}^2 + \sigma_{\text{det}}^2$, where σ_{phys} and σ_{det} are respectively the physical fluctuations and the detector resolution (see right panel of Fig. 2). Comparing data and expectations, we see that they are compatible, but the systematic error does not allow one to draw a strong conclusion on the mass composition yet.

Finally, further information about the consistency of the hadronic interaction models can be obtained by converting $X_{\text{max}}^{*\mu}$ to $\ln A$ (with A mass number), by using the following formula:

$$\langle \ln A \rangle = \ln 56 \frac{\langle X_{\text{max}}^{*\mu} \rangle_{\text{p}} - \langle X_{\text{max}}^{*\mu} \rangle}{\langle X_{\text{max}}^{*\mu} \rangle_{\text{p}} - \langle X_{\text{max}}^{*\mu} \rangle_{\text{Fe}}} \quad (3.1)$$

where $\langle X_{\text{max}}^{*\mu} \rangle_{\text{p}}$ and $\langle X_{\text{max}}^{*\mu} \rangle_{\text{Fe}}$ are the average values for proton and iron-induced air showers respectively, obtained after the reconstruction. $\langle X_{\text{max}}^{*\mu} \rangle$ is the average measured value for data. This comparison can be performed because the linear relation between $X_{\text{max}}^{*\mu}$ and $\ln A$ has been checked and verified by means of a set of Monte Carlo simulations for different nuclei. To study the systematic uncertainties, a preliminary alternative fit procedure with a stronger event selection and with a looser constraint on the USP function has been performed. This different analysis changes $X_{\text{max}}^{*\mu}$ on both data and model lines by about the same amount. The residual differences of the mass estimates when converted to $\langle \ln A \rangle$ are $\leq +0.5$. More studies on the uncorrelated systematics of the two methods need to be done in the future. Currently we conservatively add this difference in quadrature to the overall systematic uncertainties of $\langle \ln A \rangle$.

The results are shown in Fig. 4 together with $\langle \ln A \rangle$ from electromagnetic X_{max} [2], for each model separately, EPOS-LHC (left) and QGSJetII-04 (right). Considering EPOS-LHC, values of $\langle \ln A \rangle$ larger than 4 are obtained, while QGSJetII-04 provides values of $\langle \ln A \rangle$ compatible with heavy iron-like composition. This conclusion reflects that obtained for the muonic elongation rate (see Fig. 3 left) and for this analysis EPOS-LHC is disfavored. But using $\langle \ln A \rangle$ allows the comparison with different mass estimator such as X_{max} . In that case the results are not compatible both for QGSJetII-04 ($\approx 3.3\sigma$), and for EPOS-LHC ($\approx 6\sigma$). Furthermore, it should be noted that QGSJetII-04 model, unlike EPOS-LHC, has problems to describe in a consistent way the first two moments of the $\ln A$ distribution obtained from the X_{max} measurements, as discussed in [2]. Therefore, we conclude that neither of the models tuned to LHC data can satisfactorily describe at the same time both the electromagnetic and the muonic components of the showers. These are very important consistency checks for the models and from which some hadronic physics process could be excluded [7].

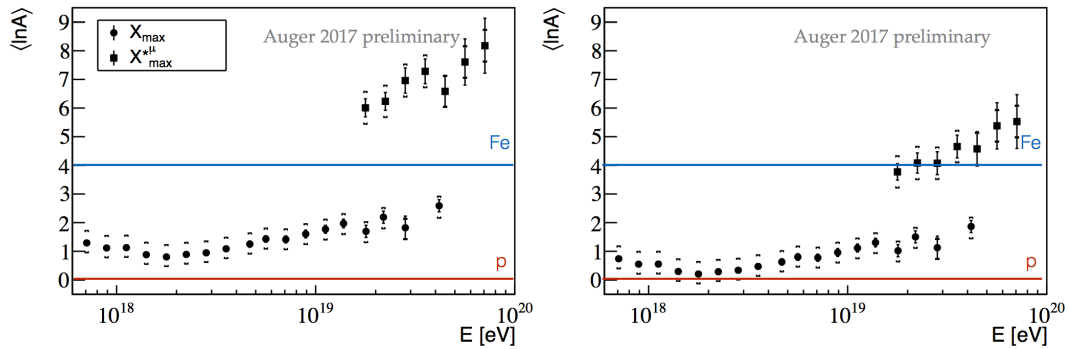


Figure 4: The evolution with energy of $\langle \ln A \rangle$ as obtained from the measured X_{\max}^{μ} (squares). The results obtained for X_{\max} (dots) [2] are also shown. EPOS-LHC (left) and QGSJetII-04 (right) are used as reference models. Square brackets correspond to the systematic uncertainties.

4. Conclusion

The arrival times of particles from EAS collected by the SD of the Pierre Auger Observatory have been exploited to measure the MPD for all events recorded in 13 years of data taking. In this work, the first two moments of the X_{\max}^{μ} distribution have been measured on extended intervals of zenith angle, energies and distances from the shower core. As a result, a large discrepancy between the EPOS-LHC hadronic interaction model and the MPD data has been found. Taking into account the mass estimated from FD measurements, the QGSJetII-04 model does not reproduce the data in a consistent way either. It is therefore difficult to make a mass composition estimation by using the MPD. However, the measurements here presented have the potential to help to understand the hadronic interactions to reduce the model systematics relevant for mass composition studies, see e.g. [13].

References

- [1] F. Fenu for the Pierre Auger Collaboration, "The cosmic ray energy spectrum measured by the Pierre Auger Observatory", in proceedings of "35th International Cosmic Ray Conference" PoS (ICRC2017) 486
- [2] A. Aab et al. (Pierre Auger Collaboration), *Phys. Rev. D* 90 (2014) 122005.
- [3] A. Aab et al. (Pierre Auger Collaboration), *Phys. Rev. D* 90 (2014) 122006.
- [4] P. Sanchez-Lucas for the Pierre Auger Collaboration, "$\langle X_{\max} \rangle$ measurements and tests of hadronic models using the surface detector of the Pierre Auger Observatory", in proceedings of "35th International Cosmic Ray Conference" PoS (ICRC2017) 495
- [5] A. Aab et al. (Pierre Auger Collaboration), *Phys. Lett. B* 762 (2016) 288-295.
- [6] T. Pierog, "Air Shower Simulation with a New Generation of post-LHC Hadronic Interaction Models in CORSIKA", in proceedings of "35th International Cosmic Ray Conference" PoS (ICRC2017) 1100
- [7] S. Ostapchenko and M. Bleicher, *Phys. Rev. D* 93 (2016) 051501.
- [8] A. Aab et al. (Pierre Auger Collaboration), *Phys. Rev. D* 90 (2014) 012012; Erratum: *Phys. Rev. D* 90 (2014) 039904(E); Erratum: *Phys. Rev. D* 92 (2015) 019903.
- [9] L. Collica, for the Pierre Auger Collaboration, *Eur. Phys. J. Plus* (2016) 131:301.
- [10] M. Mallamaci, PhD Thesis, Universita' degli Studi di Milano (2017), <http://hdl.handle.net/2434/489315>.
- [11] L. Cazon, R. Conceição, M. Pimenta, and E. Santos, *Astropart. Phys.* 36 (2012) 211.
- [12] S. Andringa, L. Cazon, R. Conceição, M. Pimenta, *Astropart. Phys.* 35 (2012) 821-827.
- [13] S. Ostapchenko, EPJ Web Conf. 125 (2016) 03013.